Mixed Aerogels from Au and CdTe Nanoparticles

*Thomas Hendel, Vladimir Lesnyak, Laura Kühn, Anne-Kristin Herrmann, Nadja C. Bigall, Lars Borchardt, Stefan Kaskel, Nikolai Gaponik, and Alexander Eychmüller**

Mixed metal–semiconductor nanocrystal aerogels are fabricated, which are light-emitting and highly porous macroscopic monoliths. Thiol-stabilized CdTe and Au nanoparticles from aqueous synthesis act as building blocks for the hybrid material. The Au colloids undergo a surface-modification to enhance the particle stability and achieve thiol functionalities. A photochemical treatment is applied for the gelation process which is found to be reversible by subsequent addition of thiol molecules. Via supercritical drying aerogels are formed. The variation of the initial CdTe to Au nanoparticle ratio permits a facile tuning of the content and the properties of the resulting aerogels. The obtained structures were characterized by means of optical spectroscopy, electron microscopy, elemental analysis, and nitrogen physisorption.

1. Introduction

In the last three decades the research on colloidal nanoparticles has evolved into a fast-growing and promising scientific area with a current focus on material sciences, biochemistry, and biophysics.[1,2] In particular, semiconductor nanoparticles (or quantum dots (QDs)) have become intensely studied objects for fundamental research and industrial use owing to their unique size dependent properties and easy processability.[3–5] They can be applied as tunable light sources in electronic, optoelectronic and photonic devices,[6–10] as well as in bio-optical[11,12] and biosensing materials.[13,14]

T. Hendel
Institut für Chemie
Humboldt-Universität zu Berlin
Brook-Taylor-Strasse 2, 12489 Berlin, Germany
T. Hendel, Dr. V. Lesnyak, L. Kühn, A.-K. Herrmann, Dr. N. Gaponik, Prof. A. Eychmüller
Physical Chemistry
TU Dresden, Bergstrasse 66b, 01062 Dresden, Germany
E-mail: alexander.eychmueller@chemie.tu-dresden.de
Dr. V. Lesnyak
Istituto Italiano di Tecnologia
Via Morego 30, 16163 Genova, Italy
Dr. N. C. Bigall
Fachbereich Physik und Wissenschaftliches Zentrum für Materialwissenschaften,
Philipps Universität Marburg
Renthof 7, 35037 Marburg, Germany
L. Borchardt, Prof. S. Kaskel
Inorganic Chemistry
TU Dresden, Bergstrasse 66, 01062 Dresden, Germany

DOI: 10.1002/adfm.201201674

In contrast to QDs, gold particles are historically known for almost 2000 years,[15] with their size-dependent optical properties and scattering effects having been explained theoretically in the beginning of the 20th century and practically proven in recent years.[16,17] Furthermore, plenty of synthetic routes have been developed in water or organic solvents[18,19] to produce gold nanoparticles with various sizes and shapes.[20,21] Gold colloids find applications in the fields of photonics,[22] surface-enhanced Raman spectroscopy,[23] biology, and medicine.[24] The interaction of QDs with metal nanoparticles has been studied intensively, as various processes like charge transfer or photoluminescence (PL) quenching and enhancement can occur, influencing the optical and catalytic properties of the designed materials, depending on their structural constitution.[25,26]

A promising new method to assemble nanoparticles into closely connected 3D networks is the formation of aerogels, highly lightweight superstructures with large specific surface areas.[27] Since the recent discovery of such porous structures built solely from colloidal semiconductor nanocrystals (NCs) like CdS,[28] progress in this field includes the fabrication of strongly emitting CdSe and CdSe/ZnS NC based aerogels with their emission spectrum resembling that of the nanocrystals themselves and hence being tunable with the NC size owing to the quantum confinement effect.[29–31] Such CdSe aerogels were already applied as selective optical sensors.[32] By using PbS nanoparticles for example, the optical activity of the resulting aerogels may additionally be adapted to the near infrared spectral region.[28] Aerogels made from thiol-capped CdTe NCs emitting green, yellow, and red light were also realized and even further hybridized with polymers to provide processability.[33] Furthermore, metal nanoparticles (Au, Ag, Pt, and Pd) were shown to be processed into gels and aerogels, and also some bimetallic aerogel structures (Au-Ag and Pt-Ag) were realized.[34,35] State of the art challenges in the field of semiconductor and metal nanocrystal aerogels are summarized in recent reviews.[31,36] All types of the reported aerogels exhibit extremely high specific surface areas in the range of 120–250 $m^2 g^{-1}$ for semiconductor[28,31] and of 30–50 $m^2 g^{-1}$ for metal based materials.[34,35] In the pioneering work of Gill et al., aerogels containing both metal and semiconductor entities were obtained throughout the controlled destabilization of CdS NCs previously modified with Ag or Au on the surface.[37,38] The design of such composite materials offers the opportunity to investigate the

very interesting interface between semiconductors and metals which allows for effective charge carrier transfer resulting in a charge separation suitable for photocatalysis[26,39] and electron storage applications.[40,41] Very recently the reversible formation of a mixed aerogel from tetrazole-stabilized CdTe QDs and gold NCs was demonstrated in which the gelation was achieved by the addition of metal ions to form a coordinated complex between the NCs.[42] Although representing a very elegant way to achieve a mixed gel formation, the introduction of a complexed metal ion between the particles avoids their close connection and could hinder the effective charge transfer in the hybrid network.

In this paper we present a different approach to form a composite metal–semiconductor aerogel built from CdTe and gold NCs. Here, photo-oxidation of the stabilizers on the NCs surface is employed to destabilize the corresponding mixed aqueous colloids. The gelation can be reversed by the subsequent addition of a thiol stabilizer analogously to the findings recently published by the group of Brock.[43] Further, the evolution of the optical properties of the formed gels is discussed and the material structure is investigated via electron microscopy, elemental analysis, and nitrogen physisorption. Due to the photochemical destabilization technique leading to close attachment of the metal and the semiconductor nanocrystals, these structures are very promising for photocatalytical applications.

2. Results and Discussion

The aqueous synthesis of thiol-stabilized CdTe NCs produces strongly emitting QDs with a narrow size distribution (see Figure S1 in the Supporting Information). UV-vis absorption and emission spectra of a CdTe QD colloid are displayed in **Figure 1**, as well as absorption spectra of the initial citrate stabilized and the gold particles functionalized with mercaptosuccinic acid (MSA). It is well known that smaller gold spheres exhibit lower colloidal stability than larger ones due to less surface charges and therefore weaker electrostatic repulsion.[44] Therefore, the MSA functionalization must be carried out carefully and in diluted NC solutions. As can be derived from Figure 1, the functionalization with MSA induced a slight shift to lower energies of the surface plasmon resonance (SPR) maximum (citrate stabilized: 508 nm; MSA stabilized: 512 nm) and its broadening, as well as a signal with increased intensity at longer wavelengths. However, no significant coalescence can be observed in transmission electron microscopy (TEM) images (see Figure S2 in the Supporting Information), so the spectral change can be attributed to the interaction of the thiol ligand with the electronic system of the Au particles. As the thiols bind via chemisorption to the Au surface, an ionic layer forms, and the concentration of free electrons in the metal core is reduced resulting in the observed damping and red shift of the SPR.[45]

In order to gel the colloidal solutions, in this work a photochemical treatment was chosen similar to the most reproducible synthesis route for gels based on aqueous CdTe NCs reported previously.[33] However, the chemical treatment with ethanol, sodium chloride, or diluted H_2O_2 solutions may also be applied, for example if it is necessary to avoid photo-oxidation.[33,34] As was shown previously, the destabilization of CdTe particles by

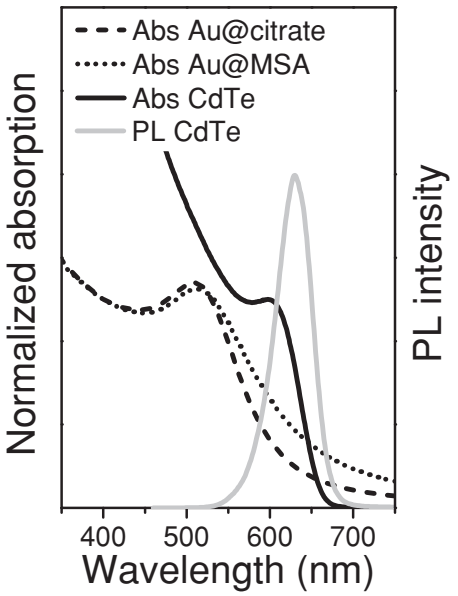

Figure 1. Absorption and PL spectra of the initial Au and CdTe NC solutions. The Au spectra were normalized to 1 at 400 nm for comparison.

the controlled removal of the ligands on the surface leads to the formation of crystalline nanowires, which retain the quantum confined properties of their colloidal building blocks.[46] For purification, we precipitated the CdTe NCs with 2-propanol and redissolved them subsequently in pure water. This can be seen as the first step of a partial ligand removal since the thermodynamic equilibrium results in a detachment of stabilizers from the particle surface. Tang et al. have demonstrated that by a prolonged storage of the diluted washed NCs in the dark a slow one-dimensional growth resulting in the formation of single-crystalline nanowires can be achieved.[46] To overcome this time-consuming self-assembly process and at the same time yield non-ordered highly porous gel-like assemblies, we applied an intensive light treatment to destabilize the NCs. The phototreatment causes a photocatalytic oxidation of the thiol ligands on the CdTe surface.[47] Brock and co-workers have shown that naked Cd atoms are detached from the crystal surface and dissolved in the solution resulting in the NC surface with high chalcogenide concentration.[43] The chalcogenides can be further oxidized under formation of chalcogenide-chalcogenide bonds serving as interparticle bridges. Furthermore, these interparticle bonds can be reductively broken by the addition of thiol stabilizers showing the reversibility of the gelation. We found that our hydrogels can be dispersed as well by the addition of thioglycolic acid (TGA), and thus we assume a similar mechanism of networking of CdTe NCs by photooxidation. Spectroscopic data further confirmed this assumption by showing emission and absorption maxima of the gels shifted to higher energies than those of the initial NC colloids that can be attributed to the solvation of Cd^{2+} ions decreasing the particle size (see Figure S3 and S4 in the Supporting Information). Several aerogel samples of different compositions presented in **Table 1** were prepared by the photochemical treatment varying the initial ratio of Au/CdTe NC colloids.

Table 1. Gelated samples with increasing amount of Au NCs and decreasing gelation time. The particle ratio and the theoretical mass ratio are calculated from the initial concentrations and the particle diameters. The resulting mass ratio was determined by EDX measurements. In the course of the further characterization, the gelated samples are named referring to this table.

Sample	Irradiation Time [min]	Particle Ratio CdTe:Au	Initial Mass Ratio Cd:Au	Mass Ratio Cd:Au [EDX] in Aerogel
G1	198	(pure CdTe)	(pure CdTe)	(pure CdTe)
G2	103	ca. 175	17.7	16.4
G3	119	ca. 65	6.7	7.4
G4	62	ca. 45	4.4	5.0
G5	45	ca. 30	3.0	3.1
G6	43	ca. 20	1.9	2.2
G7	35	ca. 10	1.1	1.4

As follows from the results obtained, the duration of the gel formation depends mainly on the proportion of CdTe NCs in the colloidal mixture. The gelation was reproducible with the necessary irradiation times ranging between 0.5 and 3.5 h decreasing with decreasing CdTe content in the mixture (see Table 1). The slight deviation of the irradiation times is acceptable as the photo-oxidation of the QDs stabilized with short-chain thiols is less reproducible than that of QDs stabilized with long-chain thiols due to a short time span between the start of the illumination and the subsequent precipitation.[47] Furthermore, it should be noted that the presence of oxygen in the colloid is an essential parameter that needs to be controlled to improve reproducibility.[47,48] Therefore, all colloids were treated under ambient conditions being flushed with air when aliquots were taken.

During the irradiation, the optical properties were monitored by UV-vis absorption and emission spectroscopy. In **Figure 2** the evolution of the absorption and PL spectra are displayed exemplarily for the mixture G3 (see Figure S5 in the Supporting Information for other mixtures). In the absorption spectra (Figure 2, left), a slight shift to higher energies of the first transition maximum can be observed, which we attribute to the above mentioned detachment and solvation of Cd^{2+} ions from the quantum dot surface by the intense radiation decreasing the nanocrystal sizes.[43,47,49] The blue shift of the spectra could also be attributed to the possible integration of sulfur into the CdTe crystal lattice. The thiol stabilizers on the surface can be hydrolyzed at elevated temperatures and intense light irradiation,[50,51] effects that cannot be excluded despite the application of a water filter and a cooling system. Due to the flocculation at the end of the phototreatment, the scattering of the solution causes a nonzero baseline signal. Additionally, particles can be removed from detection either by complete dissolution or by the formation of first small sedimenting NC oligomers. Furthermore, a lower and less pronounced absorption is found, that we attribute to the discussed overlaying scattering signal. Even in colloid mixtures with a higher gold content (see G4 and G6 in Figure S5 in the Supporting Information) a plasmonic signal cannot clearly be observed as it is strongly superimposed by the absorption of CdTe.

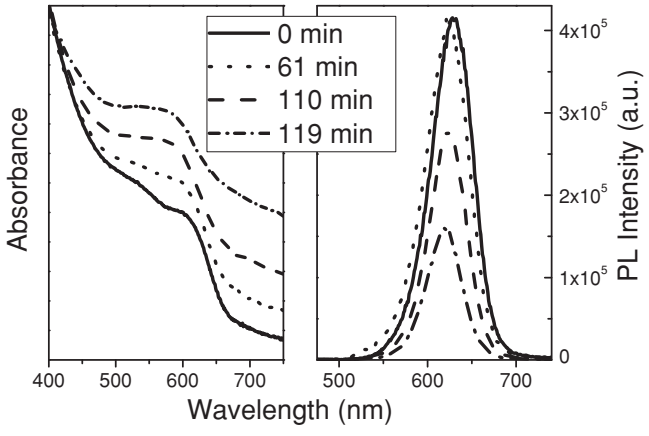

Figure 2. Absorption (left) and PL (right) spectra of the colloid mixture G3 during the irradiation. The absorption spectra are shifted vertically to achieve a clearer presentation.

The evolution of the PL spectra (Figure 2, right) displays a slight blue shift of the maximum wavelength as well as a decrease of the PL intensity. The blue shift can be related to the surface etching and the incorporation of sulfur as discussed above. A loss of PL intensity observed during the irradiation seems inconsistent with the well-known use of photoetching of QDs to enhance their PL quantum yield (PL QY)[49] but can easily be explained. Increased PL QY is achieved when unwashed solutions of thiol-stabilized CdTe NCs are used where the excess of thiols and cadmium salt in the colloid causes the formation of a protecting CdS shell around the CdTe core, while in our case the absence of free precursors enables a fast destabilization of the QDs as well as a partial degradation of the surface generating more radiationless de-excitation pathways and by this lowering the band gap emission. Furthermore, the detection of less particles due to the effects discussed above might also be responsible for a decreased PL signal. A detailed discussion on the optical properties of irradiated NCs, gels and aerogels is presented in the Supporting Information.

So far, only the spectroscopic properties of pure CdTe colloids and hydrogels (see Figure S5 (top) in the Supporting Information) have been discussed. The optical behavior of the mixed colloids and hydrogels during the photo-oxidation is drastically influenced by the interaction of the gold NCs with the CdTe QDs. The PL of the QDs can be quenched[52,53] or enhanced[54,55] depending on the distances between the metallic particle (or surface) and the QD. As in our system the gold and CdTe NCs are closely connected, the observed strong decrease of PL intensity is attributed to a charge transfer between the particles in the network acting as a nonradiative recombination pathway for the excited electrons with strong influence on the radiative relaxation pathways.

Immediately after an obvious increase in viscosity, due to the formation of small aggregates (oligomers) of NCs[31] the colloid was subjected to a slow centrifugation at 800 rpm (≈59 g). These conditions are not harsh enough to yield bulk precipitation but allow for an increase in density of the viscous colloid (approximately doubled compared to the initial value) and promote solvent expulsion. An exchange of the supernatant and

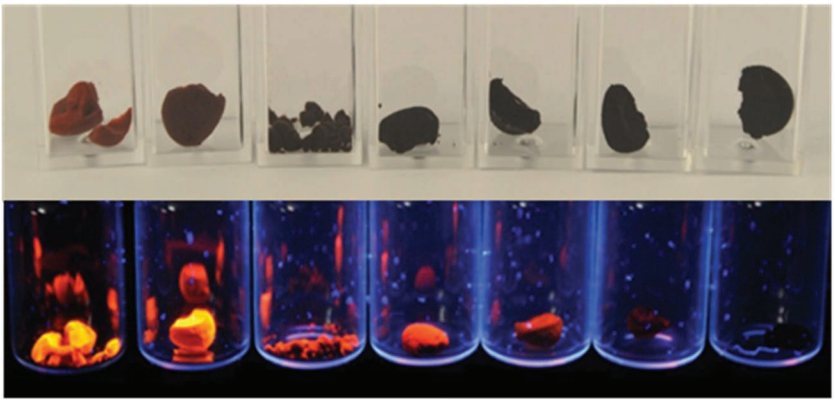

Figure 3. True color images of the aerogels G1–G7 (from left to right) with rising content of Au NCs under day light (top) and 365 nm UV-lamp illumination (bottom).

the solvent in the pores with acetone[28,33] allowed supercritical drying of the gels with CO_2 resulting in self-supporting aerogels (**Figure 3**) which show absorption and luminescence properties depending strongly on the CdTe to gold ratio. During the necessary steps for the supercritical drying the produced aerogels underwent a volume loss of approximately 30% compared to their hydrogel preforms as can be seen from photographs in Figure S6 (Supporting Information).

The morphology and composition of the resulting aerogels were investigated with scanning electron microscopy (SEM), TEM, energy dispersive X-ray spectroscopy (EDX), and nitrogen physisorption. The EDX results as displayed in Table 1 prove that the CdTe/Au ratio in the aerogel can be controlled by the initial volume ratio of the nanoparticle solutions in the mixed colloid before gelation. By SEM characterization the aerogels were found to be highly porous consisting of widely branched 3-dimensional structures interconnected with large voids in the macroporous range. **Figure 4** shows exemplarily four aerogel samples with rising gold content (for more images see Figure S7 in the Supporting Information). It can be seen that all the samples from the pure CdTe aerogel to the aerogel with the highest Au content display similar morphology of the network, indicating that the hydrogel and aerogel formation are not influenced by the ratio of the initially applied building blocks.

The porosity of the resulting aerogels was evaluated by nitrogen physisorption measurements exemplarily carried out with the aerogel sample G4 representing all mixed aerogels since the SEM imaging showed similar morphologies of the prepared gels as discussed above. The specific surface area of the sample was determined from the adsorption isotherm ($0.05 < p/p_0 < 0.2$, **Figure 5**, left) as 170 $m^2\ g^{-1}$ which is in the typical range of 120–250 $m^2\ g^{-1}$ reported for metal chalcogenide aerogels.[28,31] The pore size distribution for G4 was estimated from the desorption branch using Barrett–Joyner–Halenda (BJH) equation, and the resulting maximum of the pore size distribution was found to be at around 16 nm with a broad distribution of macropores above 50 nm (Figure 5, right), which is in good accordance with the structural properties obtained from SEM characterization and with previous aerogel characterizations.[56] A detailed discussion on the ratio of mesopores and macropores as well as bulk and skeletal densities can be found in the Supporting Information.

To reveal insight into the spatial distribution of the CdTe and gold nanoparticles, the aerogel networks were examined by TEM in detail. As can be derived from **Figure 6**, the aerogels consist of highly porous and widely branched particle networks with a statistical distribution of CdTe and Au NCs. The two different species can be distinguished in the TEM images owing to their different contrast: the gold particles appear darker and the CdTe is present as a continuous, grey, branched network. Thus, the TEM images confirm that the particle ratio in the network can be controlled by the initial colloidal mixture. From the high-resolution TEM (HR-TEM) image in Figure 6D (inset), we observe that the particles are closely connected in wire-like structures preserving their crystallinity. Further, the lattice plane distance enables for a clear identification, since we found for the Au particles distance of 2.28 Å for the [111] being in a good agreement with the literature (2.35 Å).[57] For the CdTe a lattice plane distance [111] of 3.43 Å was estimated showing a slight difference from the tabulated values for cubic CdTe (3.74 Å).[57] We assign this shift to the incorporation of sulfur into the CdTe crystal lattice during the particle synthesis[49,50] and the photochemical

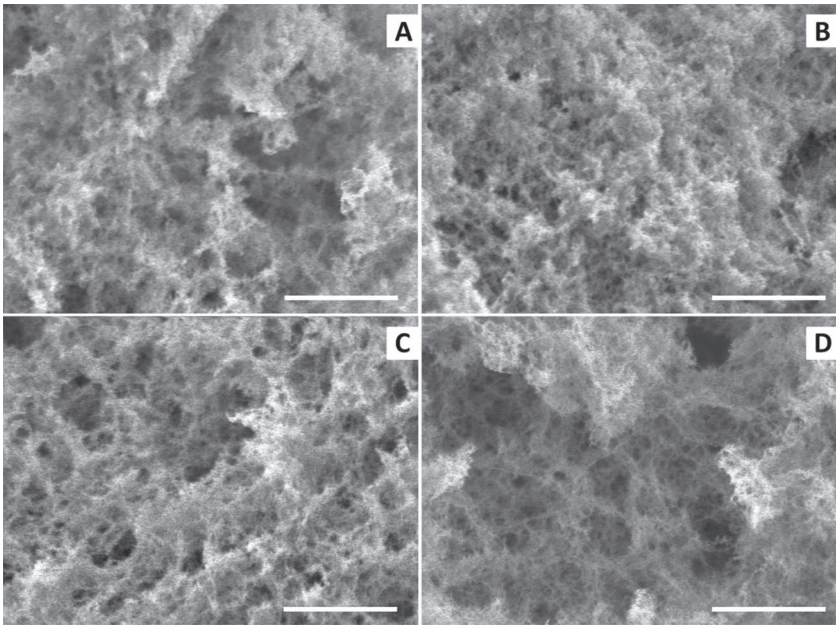

Figure 4. SEM images of mixed aerogels with decreasing CdTe/Au ratio (A, B, C, and D refer to G1, G3, G5, and G7, respectively) indicating a highly porous and homogeneous network possessing meso- and macroporous architecture. The scale bars are 1 µm.

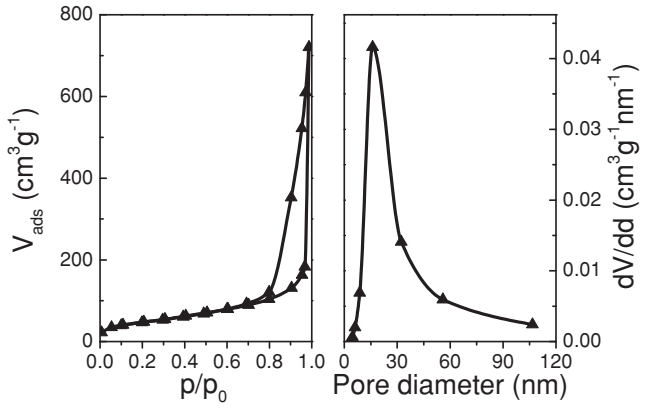

Figure 5. Nitrogen physisorption isotherm (left) for sample G4 and the related pore size distribution (right) at 77 K. Black lines are guides to the eye.

destabilization process as the unit cell of cubic CdS is smaller (3.37 Å).[57] Hence, it can be observed that the gold nanoparticle content significantly increases from sample G1 (Figure 6A) to G7 (Figure 6D, for more images see Figure S8 in the Supporting Information), which is in good agreement to the EDX analysis discussed above.

The diameter of the branches and wires displayed in Figure 6 is larger than the initial particle diameter indicating that the particles are randomly three-dimensionally interconnected when the destabilization process reaches gelation. In contrast to this observation, Tang et al. reported the slow nanowire formation with nearly similar diameters of nanoparticle and wire and a subsequent phase transition from the cubic zinc blende structure of the initial NCs to the hexagonal wurtzite type in the wires obtained.[46] The determination of the lattice plane distances from the HR-TEM images showed that our process of faster particle destabilization does not include this phase transition as the crystal lattice of the CdTe obtained in the gels can be clearly identified as cubic zinc blende type unaltered compared to the initial CdTe QDs.[4,49]

The optical properties of the resulting hydrogels and aerogels have been further investigated. From the PL spectra of the hydrogels (**Figure 7**A) it can be derived, that with an increasing amount of gold particles, the luminescence intensity of the CdTe NCs in the network decreases. This behavior is attributed to an increase of the number of excited QDs being in direct contact to gold nanoparticles, which results in an increase of the probability of the radiationless relaxation (i.e., a luminescence quenching).[38] In all gelated samples the position of the PL maximum displays a general blue shift due to the above discussed decreasing NC size and the incorporation of sulfur during the photooxidation. A comparable behavior was also found in the PL spectra of the corresponding aerogels (Figure 7B). Again, a general blue shift is observed although less pronounced than in the case of the hydrogels. To compare the PL maxima of the aerogels and the hydrogels G1-6, their average relative shift related to the PL maximum of the initial CdTe NCs (631 nm) was determined. As the hydrogels show a larger average blue shift (ca. 23 nm) than the aerogels (ca. 9 nm), we attribute this to a decreased interparticle spacing in the more compact aerogels supporting the charge transfer as well as a Förster resonance energy transfer (FRET)[58] and a reabsorption[59] that usually cause red shifting of the PL spectra. We believe that the observed deviation of the emission wavelength maxima of the various samples is related to the different shrinking behavior of the aerogels and thus based on the quality of the acetone exchange and the supercritical drying process. The slight shrinking also explains the decreased PL intensity of the aerogels in comparison to their related hydrogels, as charge/energy transfer and reabsorption effects are more favored in the aerogel networks as compared to the more expanded hydrogels. It is noted that the PL intensities of the aerogel samples with higher gold content are very weak and largely influenced by a relatively strong background signal arising from scattering and reflection effects. This may explain the rising signal below 570 nm in the PL spectra.

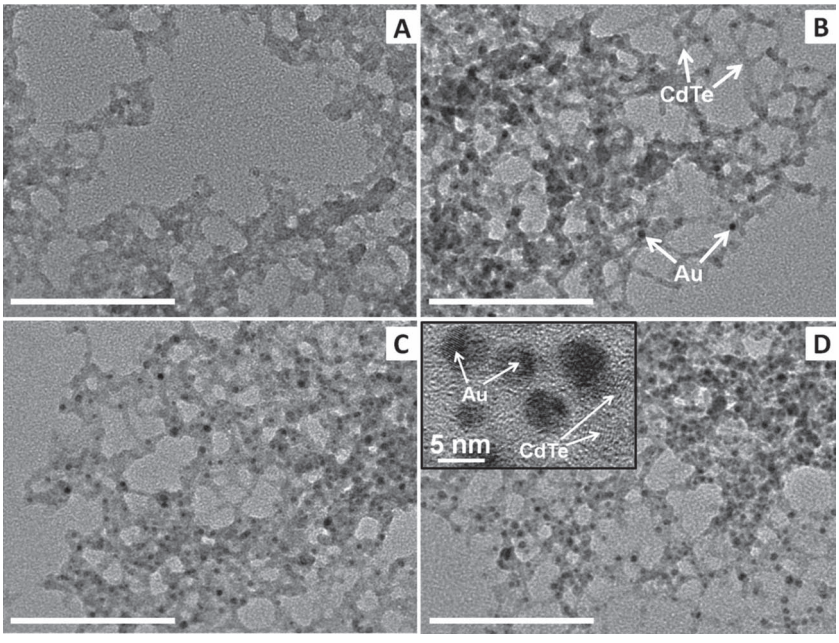

Figure 6. TEM images of four aerogel samples with rising Au NCs content (A, B, C, and D refer to G1, G3, G5, and G7, respectively). The scale bars are 100 nm. The two components can be distinguished by their different contrast (see white labels). The inset in D is a HR-TEM image showing the crystallinity of both CdTe and Au NCs in the network.

Figure 7C shows the absorption spectra of the mixed aerogels measured with an integrating sphere. The characteristic absorption band of the CdTe particles at about 580 nm is clearly pronounced for the samples with a high CdTe content. The absorption band is shifted to higher energies in comparison to the absorption of the initial CdTe NCs (598 nm, see above) due to a partial degradation of the NCs during the photo-oxidation decreasing the size of the quantum confined cores.[43,47,49] With higher gold content the

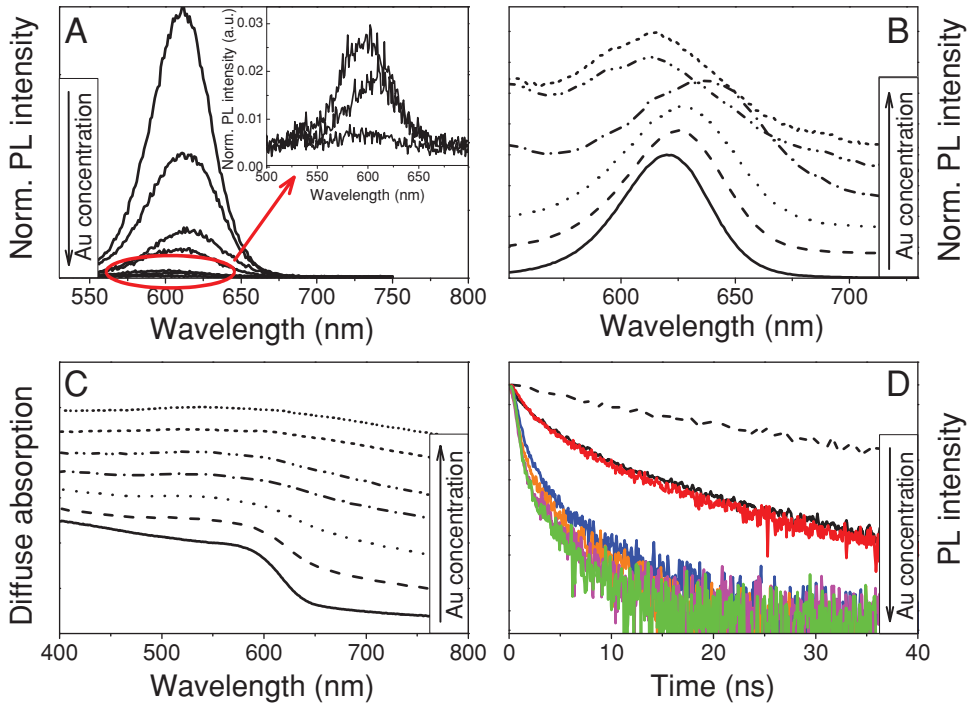

Figure 7. Evolution of the PL spectra of A) the mixed hydrogels and B) the respective aerogels, and C) the absorption spectra of the aerogels with increasing Au content. D) The PL lifetime traces of aerogels showing a decreasing lifetime with increasing Au concentration. The continuous black line and the dashed black line show the PL lifetime decays of the pure CdTe aerogel and of the initial CdTe NCs, respectively.

CdTe band gap signal is less distinguishable and the absorption spectra are dominated by a broad extinction over the whole visible area. With increasing number of metal particles dispersed in the network, they are more often located close to each other resulting in a notable optical coupling via dipole interactions. The coupling results in a red shift and a broadening of the absorption signal[60,61] which explains the black appearance of the aerogel monoliths.

Figure 7D displays the PL decay traces of the prepared aerogels. It is clearly seen that the CdTe particles in the gelated samples have shorter PL lifetimes than in their initial colloidal state (Figure 7D, dashed line) and that the PL lifetime is decreasing with increasing gold NC content in the gel network. Several processes can be responsible for the observed behavior. We assume that the fluorescence quenching through a charge transfer between the excited CdTe QDs and the adjacent Au NCs is the most dominating nonradiative pathway for the exciton. As the PL lifetime decreases notably with rising gold content, this charge transfer turns out to be effective, which is important for a possible application of the hybrid aerogels in catalytic reactions using a charged gold surface.

Hence, we point out the catalytic potential of the prepared aerogels. As was shown before, the quenching mechanism of the excited CdTe QDs through adjacent Au particles depends on the position of the valence band (VB) and the conduction band (CB) of the QDs relative to the Fermi level of the proximate Au NCs.[52] By cyclic voltammetry, the edges of VB and CB for 3.3 nm TGA-stabilized CdTe NCs were located at +0.94 V and −1.0 V related to the standard hydrogen electrode (SHE), respectively.[62,63] For the Fermi level of the Au particles (E_F) the work function of bulk gold was used, which is tabulated as +5.1 V in vacuum.[64] As the absolute electrode potential of the SHE vs vacuum is −4.44 V,[65] the Fermi level of gold vs SHE was calculated as +0.66 V. This relation is displayed in **Figure 8**

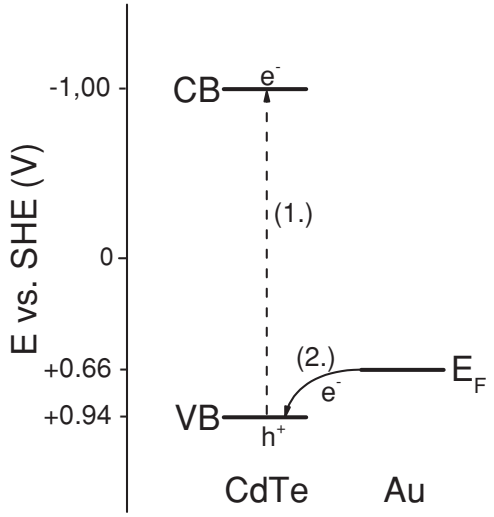

Figure 8. Energy level diagram displaying the positions of the VB and the CB band of the CdTe QDs as well as the E_F of the Au NCs. After the photoexcitation leading to the exciton formation (1.) an electron transfer from the gold to the VB of CdTe can take place (2.). The resulting local charge separation can be re-neutralized either by an electron transfer from the CB of the CdTe to the Au NC or by redox reactions on the surface of the nanoparticles.

showing that the E_F is located energetically within the band gap of the CdTe NCs, slightly above their VB. Therefore we assume that the first electron transfer is directed from the Au NC to the VB of the excited CdTe QD causing a temporary positively charged metal surface. Owing to this process hybrid aerogels are very promising materials for applications in photocatalysis for oxidation reactions on the gold surface. Experiments confirming this assumption are currently underway.

3. Conclusions

In the present work we demonstrated the controlled formation of highly porous mixed metal–semiconductor aerogels from their colloidal nanocrystalline building blocks by a reproducible photochemical treatment followed by supercritical drying. The aerogel monoliths consist of networks from homogeneously dispersed gold and CdTe nanoparticles and exhibit optical behavior dependent on their colloidal composition while retaining a number of their quantum confined properties. Materials of this type combining the optical and catalytic properties of their nano-building blocks with very high porosity of the gel structure are of special interest for applications in nanosensing and photocatalysis which will be investigated in our further work.

4. Experimental Section

Synthesis of CdTe and Au NCs, and Gel Preparation: Tetrachloroauric acid ($HAuCl_4 \cdot 3H_2O$), sodium citrate ($C_6H_5O_7Na_3 \cdot 2H_2O$), MSA ($C_4H_6O_4S$), sodium hydroxide (NaOH), sulfuric acid (H_2SO_4), isopropanol, and acetone were purchased from Sigma Aldrich. Sodium borohydride ($NaBH_4$) and TGA ($C_2H_4O_2S$) were supplied by Fluka. Aluminum telluride (Al_2Te_3) was purchased from Cerac Inc. Cadmium perchlorate hexahydrate ($Cd(ClO_4)_2 \cdot 6H_2O$) was supplied by Alfa-Aesar. All chemicals were used as received without further purification. Ultrapure deionized water was used in all preparations.

CdTe NCs were synthesized in aqueous media using TGA as a stabilizer as described elsewhere.[4,66] The synthesis resulted in stable and light emitting NCs with positions of the first absorption and PL maxima at 598 and 631 nm (see Figure 1), respectively, and with an average crystal diameter of ca. 3.3 nm.[4] In a typical synthesis, $Cd(ClO_4)_2 \cdot 6H_2O$ (4.59 g, 10.94 mmol) was dissolved in water (500 mL), and TGA (1.31 g, 14.22 mmol) was added under stirring, followed by adjusting the pH to 12 by dropwise addition of NaOH solution (1 M). The solution was placed in a three-necked flask fitted with a septum and valves and was deaerated by Ar bubbling for 30 min. H_2Te gas was generated by the decomposition of Al_2Te_3 (0.8 g, 1.83 mmol) in a separate flask with H_2SO_4 (0.5 M) and was passed through the reaction medium by a slow Ar flow for 15 min. Subsequently, the reaction mixture was refluxed under air with a condenser attached for about 24 h and then cooled to room temperature. The colloidal solution was concentrated to the solubility limit using a rotary evaporator (40 °C, 1 mbar) and precipitated by adding a small amount of isopropanol to separate unreacted species. The CdTe NCs were redissolved in pure water adjusting the concentration of this stock solution to ca. 0.04 M as determined from inductively coupled plasma optical emission spectrometry (ICP-OES) measurements. It is mentioned here that an additionally performed determination of the concentration using optical data from UV-vis and PL spectroscopy measurements of the QDs and the sizing curve predicting the size-depending extinction coefficient for CdTe NCs yielded similar concentration values as from elemental analysis, with a deviation of less than 12%.[4,67]

Gold nanoparticles were synthesized in aqueous media as well, using $NaBH_4$ as reducing and sodium citrate as capping agent[68] resulting in an average particle diameter of 3.8 ± 0.8 nm according to transmission electron microscopy (TEM) evaluation. Briefly, an aqueous solution of $HAuCl_4 \cdot 3H_2O$ (8.7 mL, 5.1 mM) was dissolved in water (150 mL) at room temperature. Shortly after, a sodium citrate solution (3.48 mL, 34 mM) was added while stirring. One minute later, 1.76 mL of a freshly prepared, ice-cooled aqueous solution of $NaBH_4$ (45 mM) and sodium citrate (34 mM) was added rapidly under vigorous stirring and finally kept for additional 5 min. The as-prepared gold nanoparticles were further functionalized with MSA via ligand exchange[69] to increase the colloidal stability and to achieve thiol functionalities on the gold surface that make the particles more suitable for a joint gelation with thiol-capped CdTe NCs. To assure efficient ligand exchange, a large excess of MSA exceeding 100 times the amount theoretically necessary to form a monolayer coverage on the NC surface (assuming a surface coverage per molecule of 0.2 nm^2)[69] was used. Therefore, in a typical preparation an aqueous solution of MSA (50 mL, 10 mM) with a pH of 6–7 adjusted by the addition of NaOH solution (1 M) was added dropwise to the citrate stabilized Au NC solution (150 mL, 2.6×10^{-4} M) under rapid stirring. The reaction mixture was kept stirring overnight in the dark.

For the gelation, the resulting colloidal solution was further concentrated and cleaned from the excess of MSA. Due to the strong ionic interactions, aqueous synthesis of gold NCs is normally performed under conditions which yield relatively diluted solutions.[70] Therefore, the solution of the thiol-capped NCs had to be concentrated further using centrifuge filters with polyethersulfone membranes with a molecular weight cut-off of 30 000 g mol^{-1} at 1500 rpm (≈362 g) and was subsequently washed twice with deionized water according to a procedure previously reported.[34] This Au@MSA stock solution had a molar gold concentration of 5 mM, as determined by ICP-OES measurements.

Stock solutions of thiol-capped gold and CdTe NCs were mixed in various ratios (see Table 1) to a final volume of 1 mL, and the gel formation was induced by photo-oxidation using a 1000 W Xe lamp, equipped with a water filter and a cooling system in order to avoid overheating. Moreover, the sample also was stirred vigorously, and the glass vial was rotated. During the gelation, which took between 0.5 and 3.5 h, aliquots (10 µL) were taken periodically to monitor changes in the optical appearance. The obtained hydrogels were further transferred into centrifuge tubes (2 mL) and centrifuged overnight at 800 rpm (≈59 g). The supernatant of the compact gel body was then carefully exchanged every 30 min against acetone (7–8 times). Finally, the hydrogels were stored for two days in a desiccator over $CaCl_2$ and water-free acetone under a reduced pressure in order to exchange the water in the pores of the hydrogel for acetone.

The hydrogels were transferred into an autoclave (critical point dryer, 13200J-AB from Spi Supplies) for supercritical CO_2 drying. The chamber was flushed with liquid CO_2 to exchange the acetone against CO_2 ($p \approx 50$ bar). After overnight storage of the gels in the autoclave at room temperature the chamber was heated up to 36 °C causing an increased pressure ($p \approx 75$ bar) and the conversion of the liquid CO_2 to the supercritical state. Finally, the CO_2 was discharged by reducing the pressure whilst keeping the temperature above the critical point to avoid capillary forces and turbulences appearing when drying is carried out under ambient conditions. Thus, the fine nanostructures were prevented from collapsing which resulted in highly porous self-supporting aerogel monoliths.[33]

Characterization: UV-vis absorption spectra of the colloids and hydrogels were recorded using a Cary 50 spectrophotometer (Varian Inc.). Absorption spectra of the aerogel samples were recorded using a Cary 5000 spectrophotometer (Varian Inc.) equipped with an integrating sphere (Labsphere Varian) for measurements of center mounted scattering samples. Fluorescence measurements were performed with a FluoroMax-4 spectrofluorometer (HORIBA Jobin Yvon Inc.). Time resolved PL traces were measured on a Fluorolog-3 spectrofluorometer (HORIBA Jobin Yvon Inc.) using a 200 ps pulsed laser diode emitting at 470 nm. For these measurements, the aerogel samples were prepared

by comminuting a piece of aerogel between two quartz glass plates. All spectra were measured at room temperature.

TEM imaging was carried out on a Tecnai T20 microscope operating at 200 kV (FEI). The samples for the TEM measurements were prepared by drop casting diluted, aqueous NC colloids or gel dispersions in methanol (previously shortly ultrasonicated) onto copper grids coated with a thin Formvar-carbon film with subsequent evaporation of the solvent.

SEM imaging and EDX analysis were carried out on a DSM 982 Gemini instrument (Zeiss). The samples for SEM were prepared by deposition of small aerogel pieces on an adhesive carbon film.

Nitrogen physisorption isotherms were acquired at 77 K using a Quantachrome Autosorb 1c apparatus. Prior to the measurement, the samples were degassed in vacuum at 423 K for 24 h. Specific surface area was calculated using the Brunauer–Emmett–Teller (BET) equation (p/p_0 = 0.05–0.2). The pore size distribution was estimated from the desorption branch using the BJH equation.

ICP-OES analysis was carried out on an Optima 7000DV instrument (Perkin Elmer). Samples for the elemental analysis were prepared by the decomposition of the Au NCs in aqua regia, while the CdTe QDs were digested by nitric acid (65%) with subsequent dilution with ultrapure water.

Supporting Information

Supporting Information is available from the Wiley Online Library or from the author.

Acknowledgements

We thank Renate Schulze for the ICP-OES measurements, Ellen Kern for the SEM/EDX characterization, Christine Mickel (IFW Dresden) for assistance in performing the TEM imaging, Ting-Ting Yang for assistance in gel preparations and Jan Poppe for discussions of energy relations between Au and CdTe NCs. This research was supported by the DFG Projects EY16/10-1, EY16/10-2 and in part by the EU FP7 NoE Nanophotonics4Energy.

Received: June 20, 2012
Revised: September 12, 2012
Published online: November 9, 2012

[1] Y. Yin, A. P. Alivisatos, *Nature* **2005**, *437*, 664.
[2] C. Burda, X. Chen, R. Narayanan, M. A. El-Sayed, *Chem. Rev.* **2005**, *105*, 1025.
[3] C. B. Murray, C. R. Kagan, M. G. Bawendi, *Annu. Rev. Mater. Sci.* **2000**, *30*, 545.
[4] A. L. Rogach, T. Franzl, T. A. Klar, J. Feldmann, N. Gaponik, V. Lesnyak, A. Shavel, A. Eychmüller, Y. P. Rakovich, J. F. Donegan, *J. Phys. Chem. C* **2007**, *111*, 14628.
[5] N. Gaponik, *J. Mater. Chem.* **2010**, *20*, 5174.
[6] P. V. Kamat, *J. Phys. Chem. C* **2008**, *112*, 18737.
[7] D. Graham-Rowe, *Nat. Photonics* **2009**, *3*, 307.
[8] D. V. Talapin, J.-S. Lee, M. V. Kovalenko, E. V. Shevchenko, *Chem. Rev.* **2010**, *110*, 389.
[9] N. Gaponik, S. G. Hickey, D. Dorfs, A. L. Rogach, A. Eychmüller, *Small* **2010**, *6*, 1364.
[10] H. V. Demir, S. Nizamoglu, T. Erdem, E. Mutlugun, N. Gaponik, A. Eychmüller, *Nano Today* **2011**, *6*, 632.
[11] I. L. Medintz, H. T. Uyeda, E. R. Goldman, H. Mattoussi, *Nat. Mater.* **2005**, *4*, 435.
[12] X. Michalet, F. F. Pinaud, L. A. Bentolila, J. M. Tsay, S. Doose, J. J. Li, G. Sundaresan, A. M. Wu, S. S. Gambhir, S. Weiss, *Science* **2005**, *307*, 538.
[13] K. E. Sapsford, T. Pons, I. L. Medintz, H. Mattoussi, *Sensors* **2006**, *6*, 925.
[14] R. C. Somers, M. G. Bawendi, D. G. Nocera, *Chem. Soc. Rev.* **2007**, *36*, 579.
[15] L. B. Hunt, *Gold Bull.* **1976**, *9*, 134.
[16] K. A. Willets, R. P. Van Duyne, *Annu. Rev. Phys. Chem.* **2007**, *58*, 267.
[17] R. Sardar, A. M. Funston, P. Mulvaney, R. W. Murray, *Langmuir* **2009**, *25*, 13840.
[18] M.-C. Daniel, D. Astruc, *Chem. Rev.* **2004**, *104*, 293.
[19] S. Eustis, M. A. El-Sayed, *Chem. Soc. Rev.* **2006**, *35*, 209.
[20] C. J. Murphy, T. K. Sau, A. M. Gole, C. J. Orendorff, J. Gao, L. Gou, S. E. Hunyadi, T. Li, *J. Phys. Chem. B* **2005**, *109*, 13857.
[21] M. Grzelczak, J. Pérez-Juste, P. Mulvaney, L. M. Liz-Marzán, *Chem. Soc. Rev.* **2008**, *37*, 1783.
[22] H. A. Atwater, A. Polman, *Nat. Mater.* **2010**, *9*, 205.
[23] L. M. Liz-Marzán, *Langmuir* **2005**, *22*, 32.
[24] R. A. Sperling, P. R. Gil, F. Zhang, M. Zanella, W. J. Parak, *Chem. Soc. Rev.* **2008**, *37*, 1896.
[25] J. R. Lakowicz, *Anal. Biochem.* **2005**, *337*, 171.
[26] P. V. Kamat, *J. Phys. Chem. C* **2007**, *111*, 2834.
[27] N. Hüsing, U. Schubert, *Angew. Chem., Int. Ed.* **1998**, *37*, 22.
[28] J. L. Mohanan, I. U. Arachchige, S. L. Brock, *Science* **2005**, *307*, 397.
[29] I. U. Arachchige, S. L. Brock, *J. Am. Chem. Soc.* **2006**, *128*, 7964.
[30] I. U. Arachchige, S. L. Brock, *J. Am. Chem. Soc.* **2007**, *129*, 1840.
[31] I. U. Arachchige, S. L. Brock, *Acc. Chem. Res.* **2007**, *40*, 801.
[32] Q. Yao, S. L. Brock, *Nanotechnology* **2010**, *21*, 115502.
[33] N. Gaponik, A. Wolf, R. Marx, V. Lesnyak, K. Schilling, A. Eychmüller, *Adv. Mater.* **2008**, *20*, 4257.
[34] N. C. Bigall, A.-K. Herrmann, M. Vogel, M. Rose, P. Simon, W. Carrillo-Cabrera, D. Dorfs, S. Kaskel, N. Gaponik, A. Eychmüller, *Angew. Chem., Int. Ed.* **2009**, *48*, 9731.
[35] W. Liu, A.-K. Herrmann, D. Geiger, L. Borchardt, F. Simon, S. Kaskel, N. Gaponik, A. Eychmüller, *Angew. Chem., Int. Ed.* **2012**, *51*, 5743.
[36] N. Gaponik, A.-K. Herrmann, A. Eychmüller, *J. Phys. Chem. Lett.* **2012**, *3*, 8.
[37] S. K. Gill, L. J. Hope-Weeks, *Chem. Commun.* **2009**, 4384.
[38] S. K. Gill, P. Brown, L. J. Hope-Weeks, *J. Sol-Gel Sci. Technol.* **2010**, *57*, 68.
[39] A. Dawson, P. V. Kamat, *J. Phys. Chem. B* **2001**, *105*, 960.
[40] G. Oldfield, T. Ung, P. Mulvaney, *Adv. Mater.* **2000**, *12*, 1519.
[41] P. V. Kamat, *J. Phys. Chem. Lett.* **2011**, *2*, 242.
[42] V. Lesnyak, A. Wolf, A. Dubavik, L. Borchardt, S. V. Voitekhovich, N. Gaponik, S. Kaskel, A. Eychmüller, *J. Am. Chem. Soc.* **2011**, *133*, 13413.
[43] I. R. Pala, I. U. Arachchige, D. G. Georgiev, S. L. Brock, *Angew. Chem., Int. Ed.* **2010**, *49*, 3661.
[44] P. Mulvaney, L. M. Liz-Marzán, M. Giersig, T. Ung, *J. Mater. Chem.* **2000**, *10*, 1259.
[45] P. Mulvaney, *Langmuir* **1996**, *12*, 788.
[46] Z. Tang, N. A. Kotov, M. Giersig, *Science* **2002**, *297*, 237.
[47] J. Aldana, Y. A. Wang, X. Peng, *J. Am. Chem. Soc.* **2001**, *123*, 8844.
[48] X. Peng, M. C. Schlamp, A. V. Kadavanich, A. P. Alivisatos, *J. Am. Chem. Soc.* **1997**, *119*, 7019.
[49] N. Gaponik, D. V. Talapin, A. L. Rogach, K. Hoppe, E. V. Shevchenko, A. Kornowski, A. Eychmüller, H. Weller, *J. Phys. Chem. B* **2002**, *106*, 7177.
[50] A. L. Rogach, *Mater. Sci. Eng., B* **2000**, *69–70*, 435.
[51] V. Swayambunathan, D. Hayes, K. H. Schmidt, Y. X. Liao, D. Meisel, *J. Am. Chem. Soc.* **1990**, *112*, 3831.
[52] B. Nikoobakht, C. Burda, M. Braun, M. Hun, M. A. El-Sayed, *Photochem. Photobiol.* **2002**, *75*, 591.

[53] J. Zhang, R. Badugu, J. R. Lakowicz, *Plasmonics* **2008**, *3*, 3.
[54] V. K. Komarala, Y. P. Rakovich, A. L. Bradley, S. J. Byrne, Y. K. Gun'ko, N. Gaponik, A. Eychmüller, *Appl. Phys. Lett.* **2006**, *89*, 253118.
[55] X. Ma, K. Fletcher, T. Kipp, M. P. Grzelczak, Z. Wang, A. Guerrero-Martínez, I. Pastoriza-Santos, A. Kornowski, L. M. Liz-Marzán, A. Mews, *J. Phys. Chem. Lett.* **2011**, *2*, 2466.
[56] S. Bag, P. N. Trikalitis, P. J. Chupas, G. S. Armatas, M. G. Kanatzidis, *Science* **2007**, *317*, 490.
[57] *CRC Handbook of Chemistry and Physics*, 84th Edition (Ed: D. Lide), CRC Press, Boca Raton, FL **2004**.
[58] A. L. Rogach, T. A. Klar, J. M. Lupton, A. Meijerink, J. Feldmann, *J. Mater. Chem.* **2009**, *19*, 1208.
[59] T. Niebling, F. Zhang, Z. Ali, W. J. Parak, W. Heimbrodt, *J. Appl. Phys.* **2009**, *106*, 104701.
[60] C. P. Collier, R. J. Saykally, J. J. Shiang, S. E. Henrichs, J. R. Heath, *Science* **1997**, *277*, 1978.
[61] T. Ung, L. M. Liz-Marzán, P. Mulvaney, *J. Phys. Chem. B* **2001**, *105*, 3441.
[62] S. K. Poznyak, N. P. Osipovich, A. Shavel, D. V. Talapin, M. Gao, A. Eychmüller, N. Gaponik, *J. Phys. Chem. B* **2005**, *109*, 1094.
[63] N. Gaponik, S. K. Poznyak, N. P. Osipovich, A. Shavel, A. Eychmüller, *Microchim. Acta* **2007**, *160*, 327.
[64] M. Cardona, L. Ley, *Photoemission in Solids 1. General Principles*, Springer, Berlin/Heidelberg **1978**.
[65] M. Archer, A. Nozik, *Series of Photoconversion of Solar Energy - Vol. 3: Nanostructured and Photoelectrochemical Systems for Solar Photon Conversion*, Imperial College Press, London **2008**.
[66] A. Shavel, N. Gaponik, A. Eychmüller, *J. Phys. Chem. B* **2006**, *110*, 19280.
[67] W. W. Yu, L. Qu, W. Guo, X. Peng, *Chem. Mater.* **2003**, *15*, 2854.
[68] K. R. Brown, D. G. Walter, M. J. Natan, *Chem. Mater.* **2000**, *12*, 306.
[69] T. Zhu, K. Vasilev, M. Kreiter, S. Mittler, W. Knoll, *Langmuir* **2003**, *19*, 9518.
[70] D. I. Gittins, F. Caruso, *Angew. Chem., Int. Ed.* **2001**, *40*, 3001.